



Investigating the effect of supramolecular gel phase crystallization on gel nucleation

Arnab Dawn,^a ‡ Marzieh Mirzamani,^a ‡ Christopher D. Jones,^b Dmitry S. Yufit,^b Shuo Qian,^c Jonathan W. Steed^{*b} and Harshita Kumari^{*a}

Received 00th January 20xx,
Accepted 00th January 20xx

DOI: 10.1039/x0xx00000x

www.rsc.org/

Abstract Supramolecular gel phase crystallization offers a new strategy for drug polymorph screening and discovery. In this method, the crystallization outcome depends on the interaction between solute and gel fibre. While supramolecular gels have shown success in producing new polymorphs and crystals with novel morphologies, role of the gel and nature of gel-solute interaction remains largely unexplored. The present study aims to provide a comprehensive picture of the structural evolution of a supramolecular gel produced from a bis(urea) based gelator (**G**) in the presence of a polymorphic drug carbamazepine (CBZ). The structural aspects of the gel have been assessed by single crystal X-ray analysis, X-ray powder diffraction (XRPD) and solid state NMR spectroscopy. Small Angle Neutron Scattering (SANS) has been used to follow the changes in gel structure in the presence of CBZ. Visual evidence from morphological study and structural evolution observed at a macroscopic level from rheological measurements, shows good agreement with the SANS results. The Concentration of the gelator and the relative proportion of **G** to CBZ were found to be crucial factors determining the competitive nucleation events involving gelation and crystallization. At a critical **G** to CBZ ratio the effect of CBZ on gel structure was maximum and fiber bundling in the gel was found to be critically affected. This study offers important information about how the interplay of gelator assembly and gel-solute interactions can fine-tune the nucleation events in a supramolecular gel phase crystallization.

Introduction

Supramolecular gel phase crystallization using low molecular weight gelators (LMWG) offers an alternative new strategy to polymorph discovery in comparison to the conventional solution phase processes in which the gel fibers can potentially act as template for the discovery of novel solid forms.¹ The processes of supramolecular gelation and crystallization both stem from nucleation, a molecular process where a critical number of molecules are needed to achieve the phase change from melt or solution into a gel fiber or a crystal. Classical nucleation theory envisages an ordered particle in which growth becomes favourable beyond a critical radius. Two-step nucleation theory regards the crystallization process as occurring via a dense fluid phase.² In both gelation and crystallization, nucleation from a supersaturated solution is likely to have similar characteristics. Subsequent growth of

crystals occurs in a three-dimensional fashion (although preferential growth in one direction can be seen in some cases)³ whereas in gelation, particles grow rapidly in a one-dimensional fashion to give fibrils, and subsequently entangle to form a three-dimensional network structure.⁴ Growth of crystals within supramolecular gels is a time-resolved process in which the gelation occurs before the subsequent crystallization of a dissolved substrate. Gel-grown crystals can exhibit improved physical characteristics as a result of the suppression of convection currents and sedimentation afforded by the viscous gel environment. In many instances the gel is considered to act as an inert matrix within which crystal growth occurs, however in specific cases, the gel structure is capable of influencing both polymorphic form and crystal habit.⁵ There have been recent attempts to specifically design supramolecular gelators in order to promote gelator-substrate interactions and hence influence the outcome of a gel phase crystallization process.^{5b,5d} However, it is still hard to understand the detailed interactions of solutes with gel fibers and hence rationally design suitable gelators that can interact strongly with molecular species such as pharmaceuticals. In addition, it is not clear how the presence of a particular solute can influence the nucleation and growth of the gel itself. Studies on the effect of additives on the supramolecular gelation are not unprecedented. There were reports on small molecular additives where the added substrates were either gel forming components to assist the gelation of the primary

^a College of Pharmacy, University of Cincinnati, Cincinnati OH 45267-0004, USA
E-mail: kumariha@ucmail.uc.edu

^b Department of Chemistry, Durham University, Lower Mountjoy, South Road, Durham DH1 3LE, UK

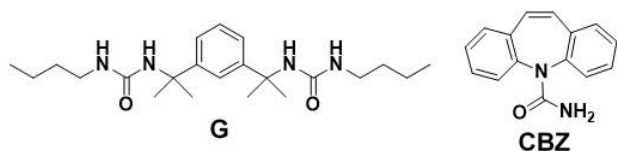
E-mail: jon.steed@durham.ac.uk

^c Oak Ridge National Laboratory, USA

† Electronic Supplementary Information (ESI) available: [details of any supplementary information available should be included here]. See DOI: 10.1039/x0xx00000x

‡ Contributed equally

gelator, or the non-gelling substrates to only modify the primary gelation.⁶ More recently, polymer additives have also been used to fine-tune the physicochemical properties of supramolecular gels.⁷ However, there have been very attempts to obtain structural information during the growth of a supramolecular gel especially when fine-tuned by the presence of crystalline substrate within it. While electron microscopy and wide-angle X-ray scattering techniques can give visual and some structural information on gels, or more commonly xerogel structure, they are unable to give insight into the solute-solvent interplay that dictates fibre growth and self-assembly.



Scheme 1. Structure of gelator **G** and the drug carbamazepine (CBZ) used in the study.

The present study attempts to address the process of nucleation in a supramolecular gel system, in the presence and absence of a polymorphic drug molecule primarily using small angle neutron scattering (SANS) as a tool for monitoring the size and shape of the growing gel fibers in a quantitative manner. The advantages of SANS over small angle X-ray scattering (SAXS) are its sensitivity towards lighter elements and scope for isotope labelling. Using deuterated solvents in SANS provides good contrast to extract meaningful structural information on the gelator. Labelling is difficult to achieve with SAXS since it involves heavy atom labelling which drastically changes the sample. Unlike SAXS where one can measure only density fluctuations, the deuteration method in SANS allows one to measure both density and compositional fluctuations. SANS uses elastic neutron scattering at small scattering angles to capture the structure of various substances at a scale ranging from 1 nm to 1000 nm. Thus, SANS could be an important tool to shed light on growth process of the gel fiber. The relatively high cost of neutron beam time together with the complexity involved in data modelling and analysis, however, means that reports of SANS studies on supramolecular gel systems are rather limited.⁸ In our recent work comparing fluorinated and non-fluorinated bis(urea) LMWGs, we were able to elucidate the evolving structural profile of both systems at varying concentrations, solvents and temperatures.^{8f}

In the present work, a simple bis(urea) gelator (**G**, Scheme 1) was chosen to form the gel for crystallization study. Gelator **G** is readily prepared in one-step from the appropriate diisocyanate and *n*-butylamine (see Experimental Section). The compound is a highly efficient organogelator (a supergelator), capable of gelling aromatic solvents such as toluene and 1,2-dichlorobenzene at a concentration below 0.1 w/v.

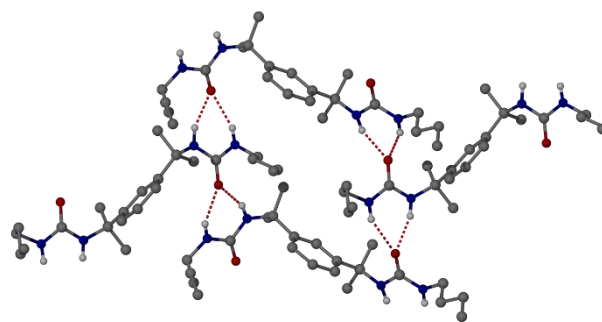


Figure 1. Single crystal X-ray structure of **G** showing the [AB] repeat unit, and antiparallel arrangement of urea α -tape hydrogen bonded motifs (CH hydrogen atoms omitted for clarity). Hydrogen bonded N \cdots O distances: 2.82 – 2.92 Å.

Carbamazepine (CBZ), an anticonvulsant, was selected as a model drug substrate based on a number of previous studies involving gel-phase crystallization of this substance.^{5a, 9} CBZ can exist in five polymorphic forms, of which Form III is thermodynamically the most stable under ambient conditions.¹⁰ Forms I-IV are all based on cyclic hydrogen bonded dimers while the catameric Form V is only accessible via epitaxial overgrown on a dihydrocarbamazepine seed crystal.¹¹ Rheology and morphological investigations were performed to support and complement the SANS analysis. In addition, solid-state NMR spectroscopy, powder and single crystal X-ray analysis of **G**, provide important insights into the structures of the materials.

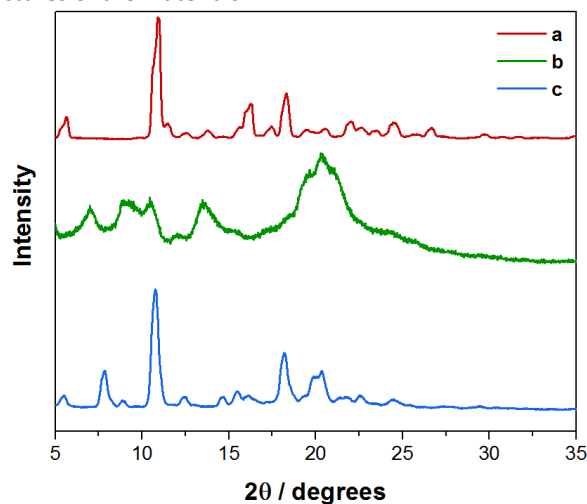


Figure 2. XRPD patterns for ground single crystals of **G** (a), a dried 1% (w/v) gel of **G** from toluene (b), and the same xerogel after heating at 100 °C for 48 h (c).

Results and Discussion

Gelator Structure

Insight into the aggregation of **G** was obtained from a single crystal X-ray structure using a crystal obtained by slow cooling of a hot solution of the compound in methanol. The X-ray crystal structure is shown in Figure 1. The compound adopts a lamellar hydrogen bonding network with a simple [AB] repeat unit. Molecules are linked by a pair of anti-parallel urea α -tape hydrogen bonded motifs with the two NH \cdots O interactions in each six-membered hydrogen bonded ring being relatively

short and similar to one another as typically observed in bis(urea) gelator structures.¹²

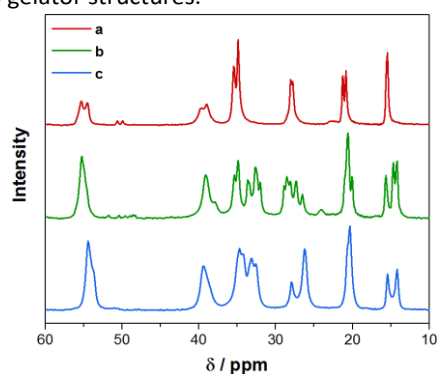


Figure 3. Solid-state ^{13}C NMR spectra in the sp^3 region ($\delta_c = 10\text{--}60$ ppm) for single crystals of **G** (a), xerogel prepared from a 1% (w/v) gel in toluene (b), xerogel after heating to 100 °C for 48 h (c).

In order to correlate and compare the single crystal and gel structure, single crystals and toluene xerogels of **G** were analyzed by X-ray powder diffraction (XRPD) and solid-state MAS ^{13}C NMR spectroscopy. Broad peaks in the XRPD pattern of the xerogel do not match reflections in the XRPD pattern calculated from the single-crystal data, suggesting that the structures of **G** in gel and crystal are significantly different (Fig. 2). Intriguingly, heating at 100 °C for two days causes the XRPD pattern of the xerogel to become sharper, indicating that recrystallization has taken place and the XRPD patterns more

closely resembles that of the crystalline material.

The solid-state ^{13}C NMR spectra confirm that the alkyl end groups in the heated material and parent xerogel experience similar local environments, but are packed differently to those in the single crystals (Fig. 3). The spectrum for single crystals of **G** displays sharp doublet peaks corresponding to the two halves of the molecule in the asymmetric unit. The xerogel prepared from a 1% (w/v) gel in toluene also produces sharp resonances, indicative of locally ordered and immobile assemblies, but there are more peaks likely due to a greater variety of conformations present. Heating the xerogel to 100 °C or 48 h leads to coalescence of the signals, suggesting that recrystallization has taken place. The terminal methyl resonances of the xerogel and recrystallized solid are shifted up-field relative to that of the single crystals.

SANS

Gel samples were studied using SANS in the presence and in the absence of CBZ at a fixed concentration of 0.2% w/v, and at three different concentrations of **G** (0.06%, 0.12%, and 0.25% w/v). The low CBZ concentration was chosen to minimize the interference of the resulting macroscopic CBZ crystals on the signals arising from the gel network. SANS measurements were carried out in deuterated solvent (toluene- d_8) to improve the scattering contrast between solute and the solvent thereby improving the coherent scattering of

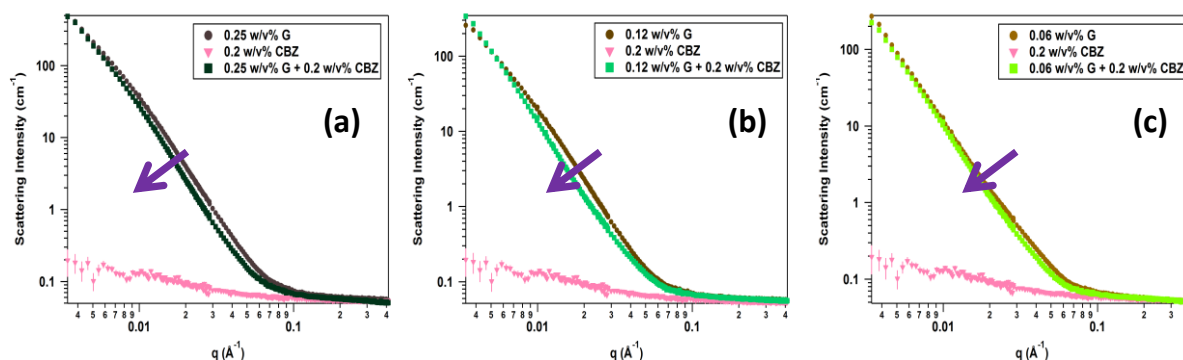


Figure 4. Overlays of SANS curves of gel alone, CBZ alone and gel with CBZ for varying concentrations of the gelator **G**, (a) highest **G** concentration, (b) medium **G** concentration and (c) lowest **G** concentration.

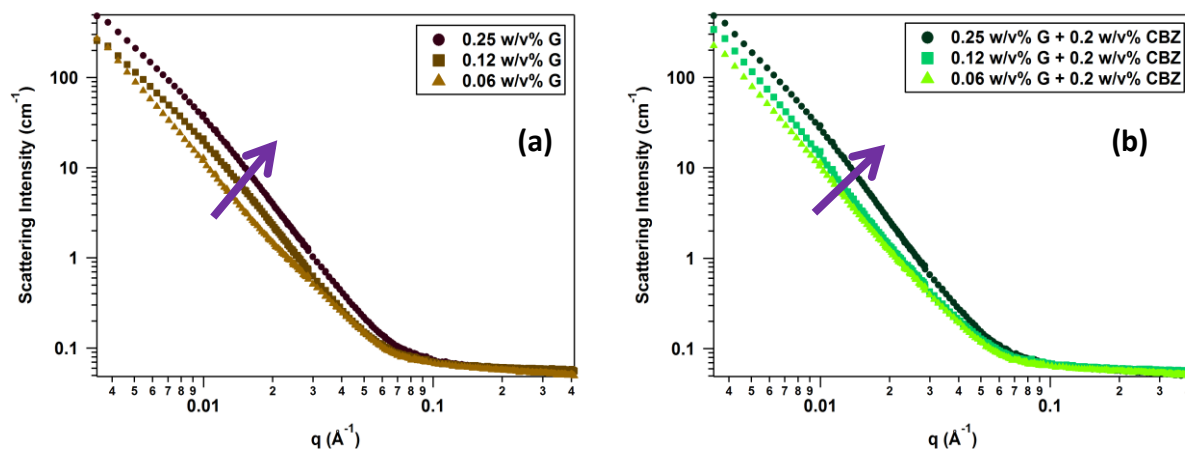


Figure 5. SANS overlays of gel samples as a function of concentration in the (a) absence and (b) presence of 0.2 wt% CBZ

neutrons which embeds the structural information.

Overlays of SANS curves of gel alone (**G**), drug alone (CBZ) and gel with drug (**G**-CBZ) as a function of gel concentration show that the scattering intensity from the gel slightly decreases when the drug molecule is present (Fig. 4), suggesting an alteration of the gel structure after adding the drug.

Overlays of SANS curves of increasing gel concentrations in the presence and absence of drug shows increasing scattering intensities, indicative of more extensive density fluctuations as the gel concentration increases (Fig. 5). This can be interpreted as a development of denser fibrous structure as gelator concentration increases. In contrast, the presence of drug results in a noticeable increase in scattering intensity only for the 0.25% (w/v) gel, indicating that a higher concentration of **G** is needed for overcoming the influence of drug in fibrous structure formation.

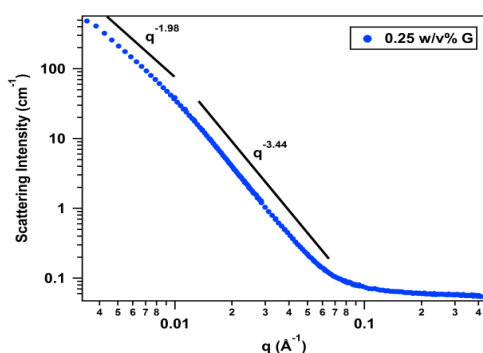


Figure 6. Example of inverse power law exponents for the high- and low- q regions of 0.25 w/v% **G** only

SANS data for **G** and **G**-CBZ were reduced and fitted to a number of models, including the modified correlation length, Guinier-Porod, dilute lamellar and fractal flexible cylinder models (Supporting Information). Resolution-smear models were used to take into account factors such as apertures, instrumental geometry, wavelength spread and effect of gravity on neutron trajectory. Unlike the previously-studied fluorinated and non-fluorinated bis-urea gelators (fitted to fractal flexible cylinder and Gaussian peaks models),^{8f-g} specific scattering features are lacking in the current data. We therefore determined the inverse power law exponents of the slopes (in IgorPro^{13a} software) to understand the structures' fractal geometry, and we used the so-called Gel Fit Model (in SasView^{13b}) to gain further knowledge of the gel fibers and aggregates.

Each SANS data set consists of two slopes, an example of which is shown in Fig.6. General information on the structure of the system, such as if the scattering entity is a sphere or a cylinder, can be obtained by determining the power law exponent of the scattering intensity decay, $I \sim q^{-n}$.¹⁴ In some cases, n is a fractional power, which would indicate that the system exhibits self-similarity over increasing length scales and is therefore a fractal. A decay of q^{-2} is indicative of a thin disk or Gaussian polymer chains whereas q^{-1} is indicative of a rod like structure. The 0.25 w/v% **G** data for example shows that I decays as $q^{-1.98}$ over the low- q region and $q^{-3.44}$ over the high- q

region (Fig.6). **G** is expected to form cylindrical fibers (the fibrous structure has been confirmed by SEM, *vide infra*) given its molecular structure and available hydrogen bond forming sites in the monomer. The $q^{-1.98}$ behavior at large length scales suggests that there is extensive bundling and irregular branching.¹⁵ The scattering intensity for a three-dimensional surface fractal decays as $I \sim q^{-(6-d_s)}$, where the surface fractal dimension d_s falls between 2 for perfectly smooth surfaces and 3 for surfaces rough enough that they are indistinguishable from mass fractals.¹⁴ The high- q decay of $q^{-3.44}$ indicates surface scattering with a d_s value of 2.55, suggesting that the fiber surfaces are quite rough. It is reasonable to consider that bundling of fibers in **G** owing to the van der Waals interactions could contribute to the roughness.

Table 1 shows the slopes of the scattering data and surface fractal dimensions for all six gel samples. The low and mid-high slopes of the 0.06 w/v% **G** concentration were essentially nonvariant indicating that the structure is highly self-similar over a wide length scale. Self-similarity in this context means that a small mass-fractal network at a short length scale that is as disordered as the overall network structure seen at a longer length scale.^{15b,c} On the contrary, the low and high q slope values for 0.12 and 0.25 w/v % **G** only samples are different indicating absence of self-similarity with increase in concentration. The difference in low and high q slope values for different concentrations of **G** suggests an increase in bundling and cross-linking at higher concentrations (Table 1).

Unlike the gel alone sample, structural variations differ in gel samples with CBZ. The reason behind this contrasting trend could be the presence of binary nucleation involving **G** and CBZ versus **G**-only nucleation event. In the presence of fixed CBZ concentration (0.2 w/v%), the 0.06 and 0.12 w/v% samples show similar low- and high- q slope values, indicating that there was little variation in the bundling, roughness and connectivity of fibers. Influence of drug crystallization on fiber entanglement could be the cause of this levelling effect, particularly at a higher drug to gelator ratio.

	Low- q Slope (-)	Mid-High- q Slope (-)	Surface Fractal Dimension
0.25 w/v% G	1.98	3.45	2.55
0.12 w/v% G	2.04	3.41	2.59
0.06 w/v% G	2.82	2.99	3.01
0.25 w/v% G + CBZ	2.26	3.51	2.49
0.12 w/v% G + CBZ	2.54	3.20	2.80
0.06 w/v% G + CBZ	2.48	3.08	2.92

Table 1. Slopes of the low- and high- q regions and the surface fractal dimension determined by the high- q slope for gel samples with varying concentration in absence and in presence of 0.2 % (w/v) CBZ.

The low and high q slope values of the 0.25 w/v% **G** + 0.2 w/v% CBZ data, on the other hand, indicate a higher density of aggregates (Table 1). The addition of CBZ to 0.25 w/v% **G** made the fiber surface slightly rougher ($d_s = 2.49$) while increasing the size of the bundles and amount of branching compared to

the 0.25 w/v% **G** alone. Adding CBZ to the 0.12 w/v% **G** gel resulted in a marked increase in the fiber roughness and amount of branching ($ds = 2.80$). Adding CBZ to the 0.06 w/v% **G** gel caused a noticeable change in the gel structure: surface scattering from extremely rough fiber surfaces ($ds=2.92$) was observed, while the amount of branching decreased and the rigidity of the fibers increased to some degree (Table 1). The existence of surface scattering indicates that significant number of fibers were packed densely to form bundles,^{15c} unlike the 0.06 w/v% **G**-only sample which only had a small fractal network. Therefore, presence of CBZ is critically affecting the course of fiber entanglement in gelation event based on the relative proportions of **G** and CBZ in the system.

The gel data were then fit to the Gel Fit Model in SasView (example shown in Fig.7). The fine scale distribution in a gel involves two length scales characteristic of gels: namely, a shorter correlation length (a_1) related to the positions of the fibers to describe rapid fluctuations that ensure thermodynamic equilibrium, and a longer correlation length (a_2) related to the positions of the clusters where the fibers are gathered together accounting for static accumulations by junctions/clusters.^{15d} The equation for the model used is the generalized form,^{15d,e,f}

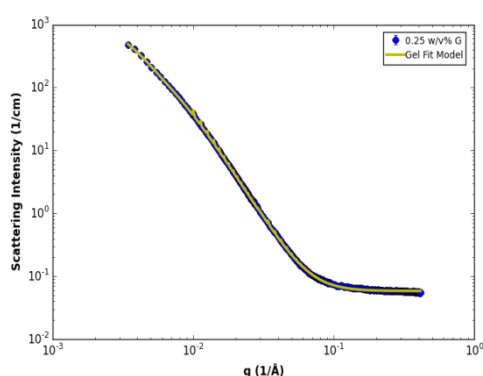


Figure 7. Example of the Gel Fit Model fit to the 0.25 w/v% **G** data.

$$I(q) = \frac{I(0)_L}{\left(1 + \left[\left(\frac{D+1}{3}\right)q^2 a_1^2\right]^{D/2}\right)} + I(0)_G \exp\left(-q^2 \frac{R_g^2}{3}\right) + B,$$

where $\frac{R_g^2}{3} \approx a_2^2$, R_g is the radius of gyration for the clusters, D is the fractal dimension of the fibers, $I(0)_L$ and $I(0)_G$ are the Lorentzian and Guinier scales respectively, and B is the incoherent background. Structural parameters obtained from the Gel Fit Model for each sample are shown in Table 2. For the **G**-only samples, variation of $I(0)_G$ and R_g indicate that the number and size of the fiber bundles increase as the concentration of **G** increases.

To better understand the effect of drug on gel nucleation, the drug only data was subtracted from gel+drug data and then fitted to Gel Fit Model. The fiber correlation length decreases as the gel concentration increases suggesting that the fibre network becomes more complex and branched with increase in gel concentration. Interestingly, the drop in

correlation length is much steeper from 0.06 w/v% to 0.12 w/v% (68%) than from 0.12 w/v% to 0.25 w/v% (5%). This means a secondary assembly involving fiber entanglement becomes significant at a concentration higher than for 0.06% (w/v). In the presence of CBZ a similar trend is observed; however, the drop in correlation length is much less impacted from 0.06 w/v% to 0.12 w/v% (1%) than from 0.12 w/v% to 0.25 w/v% (49%). This means that in the presence of CBZ desired complexity in the fibrous structure attends at a much higher concentration of **G**, where the influence of CBZ nucleation is outweighed by the higher abundance of **G**. The shift in threshold concentration from 0.12 w/v% (gel only) to 0.25 w/v% (gel with CBZ) is consistent with both Gel Fit Model and inverse power law exponents of the slopes.

Sample	Lorentzian/Guinier Scale ratio, $I(0)_L/I(0)_G$	R_g (Å)	Fiber Correlation Length (Å)
0.25 w/v% G	0.57	753.36	161.12
0.12 w/v% G	0.67	754.27	170.00
0.06 w/v% G	155.90	329.82	535.74
0.25 w/v% G + CBZ	0.88	698.45	184.90
0.12 w/v% G + CBZ	289.44	279.30	360.90
0.06 w/v% G + CBZ	155.95	211.01	364.15

Table2. Structural parameters of gel systems with varying concentration without and with 0.2% (w/v) CBZ, from the Gel Fit Model

The $I(0)_L/I(0)_G$ ratio for the 0.06 w/v% **G** sample is also extremely large, suggesting that most of the scattering is from the non-cross-linked fibers.^{15d} The $I(0)_L/I(0)_G$ ratio then drops sharply when the concentration reaches 0.12 w/v%, further suggesting that the added gelator induces cluster growth. A very slight drop in $I(0)_L/I(0)_G$ ratio from 0.12 w/v% to 0.25 w/v% indicates a near saturation of cluster formation. The trend is more inconsistent in presence of CBZ. The R_g values for the gel samples with or without CBZ increase with increasing concentration of **G** indicating cluster formation. Interestingly, as we observed previously the cluster formation is shifted toward a higher concentration of **G** in presence of CBZ.

Morphology

The morphology of the xerogel samples with or without the drug molecule was studied by SEM. The gel appeared to be fibrous in nature (Fig.8 and Supporting Information Fig.S1) with an increase in bundling with the increasing concentration of **G**. Interestingly, the **G**-CBZ sample shows the presence of both gel fibers and CBZ crystals in well defined, separated regions in the case of the (0.12% w/v) sample. The region with CBZ crystals (Fig.8b) shows less bundling compared to the region without any CBZ crystals (Fig.8a). Simultaneous formation of fibril/bundle and crystals is less abundant in the gel with 0.06% (w/v) **G** in presence of CBZ (Supporting Information Fig.S1). In case of 0.25% (w/v) gel in presence of CBZ on the other hand shows substantial amount of CBZ

crystal over the fully grown entangled gel fibers (Supporting Information, Fig.S1). Therefore, it appears from the morphological study that the presence of CBZ is inhibiting or slowing down the fibril formation and/or bundling, and such an influence from CBZ is less operative in presence of higher amount of **G**.

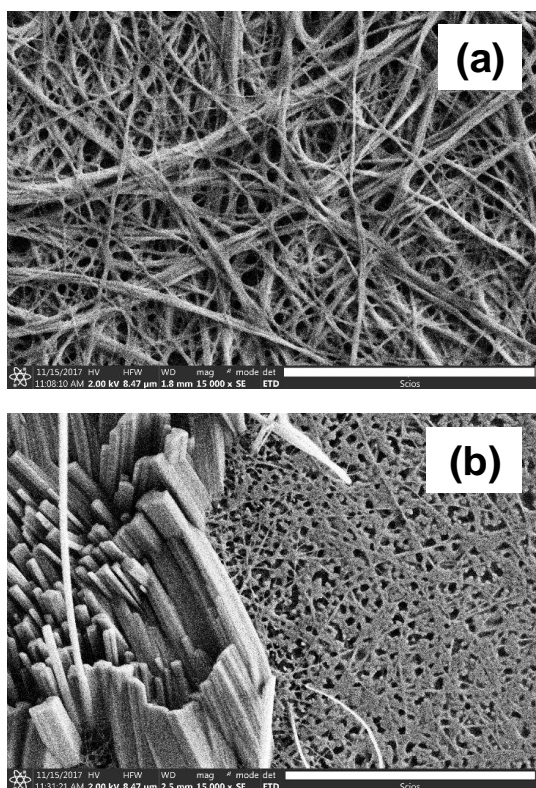


Figure 8. SEM images of the xerogel samples prepared from toluene: (i) 0.12% (w/v) gel of **G**, (ii) 0.12% (w/v) of **G** in presence of 0.2% (w/v) CBZ (Scale bars shown in the figure represent 4 μm).

Rheology

The viscoelastic properties of gel samples with and without CBZ, were examined following the same sample preparation conditions used for SANS study. All the experiments were carried out at 25°C, using toluene as the solvent for gel preparation. In order to estimate linear viscoelastic region of the samples, stress-sweep experiments were performed at a constant frequency of 1 Hz. Storage (G') and loss moduli (G'') were plotted against increasing oscillation stress (Fig.9, and Supporting Information Figure S2). In the linear region, G' proved to be much greater than G'' for all six samples (Supporting Information Figure S2), which confirms the system as more elastic than viscous, a typical characteristic of supramolecular gels.^{4g, 16} The yield stress values are summarized in Fig.9. As expected, the yield stress values increase with increasing gel concentration both in the absence and presence of CBZ. Addition of CBZ lowers the yield stress values for all three concentrations. However, for the most concentrated gel (0.25% w/v), the effect of addition of CBZ on yield stress value is least. Very interestingly, for the gel with concentration 0.12% (w/v) the change of yield stress value upon addition of CBZ is the most significant, while an

intermediate effect is observed for the weakest gel (0.06%, w/v). In the frequency-sweep experiments, all the gel samples, with or without CBZ appeared to be practically independent of frequencies (Supporting Information Fig.S3). This signifies a more permanent nature of the network structure within the timescale of rheological experiments, a characteristic of robust gel systems.

Influence of CBZ on structural evolution of the gel

From the above discussion, the following findings can be summarized: (i) Supramolecular gelation involving **G** alone is a sequential process where the bundle formation via fiber entanglement takes place once the fiber density becomes significantly high. This saturation point can be achieved easily in a gel system with a higher concentration of **G**; (ii) Presence of

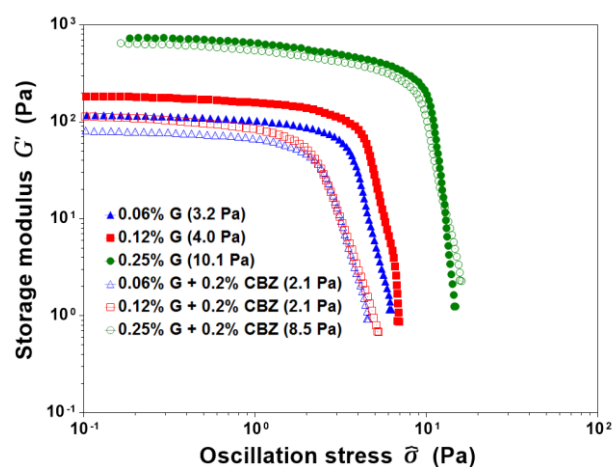


Figure 9. Stress-sweep experiments performed at a constant frequency of 1 Hz on different gel samples (with and without CBZ) prepared in toluene, at 25 °C. Shown in brackets are the yield stress values calculated from the plots.

CBZ influences the structural evolution of the gel in a complex way where inter-fiber interaction leading to the bundle formation is crucially retarded/suppressed; (iii) Relative proportions of **G** and CBZ play critical role.

The above finding can be rationalized based on the competitive nucleation involved in gelation and in crystallization events. **G** is crystalline in nature as evident from the single crystal study (Fig. 1). Moreover, **G** is transformable from one crystalline form to another as it appeared from the high temperature XRPD (Fig. 2) and solid state NMR (Fig. 3) studies. Although the structural arrangements of **G** in the crystal (formed in methanol) and in the gel (formed in toluene) are distinct, because of its crystalline nature **G** can potentially act as an efficient epitaxial surface for CBZ crystallization, and at the same time the presence of CBZ can influence the structural evolution of gel. With increase in gel concentration nucleation of gel fibrils will become faster. In contrast, with an increase in gelator concentration diffusion rate or convection will be suppressed, and in turn nucleation of CBZ may slow down. Considering above factors it is reasonable to consider that at the lowest gelator concentration when the relative

abundance of CBZ and medium convection both are highest, nucleation of CBZ is faster than gel nucleation. Conversely, for the gel with highest gelator concentration, when the medium convection is lowest gel nucleation is much faster than the CBZ nucleation. In both situations, the effect of CBZ is less pronounced. However, for the intermediate concentration of gel (0.12%, w/v), the nucleation rates of gelation and crystallization are more comparable and competitive that they influence each other. This might be the reason for the marked changes in different parameters at this medium concentration (0.12% w/v) as observed from SANS and rheological studies. This is also reflected in the local morphology of 0.12% of the gel in presence of CBZ, where crystals and immature gel fibrils are present simultaneously. Therefore, the crystallinity of the gelator molecule, gelator concentration, and relative proportions of gelator vs. substrate all have crucial role in supramolecular gel phase crystallization.

Conclusions

In conclusion, the present study reveals that in a gel-phase crystallization, the nucleation of the gelator and solute occur primarily in an orthogonal fashion with minimal interaction between the gel fibres and crystallizable target. However, under a specific set of conditions when both nucleation events occur simultaneously in competitive manner, the solute can give rise to significant changes in gel strength and structure. Competitive nucleation events involving gelation and crystallization were found to be driven by the gelator concentration, and the relative proportion of gelator vs substrate. These insights will help to optimise the conditions for supramolecular gel phase crystallization and highlight the critical interplay between tie-resolved non-equilibrium self-assembly processes in these systems.

Experimental

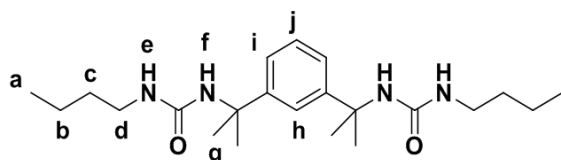
Materials

All the reagents were purchased from Sigma-Aldrich. Solvents were purchased from Fisher Scientific. Deuterated solvents were purchased from Cambridge Isotope and Sigma-Aldrich.

Single-crystal X-ray diffraction

Crystals of suitable quality for single-crystal X-ray diffraction were obtained by slow, partial evaporation of a 1% (w/v) methanol solution under ambient conditions. Diffraction data were collected at 120 K on a Bruker D8 Venture (CMOS area detector) using MoK α radiation ($\lambda = 0.71073$ Å). Data were processed using the Bruker APEX II software and solved and refined using the SHELX suite of programs¹⁵ in Olex2.¹⁶

Synthesis of gelator G



To a stirred solution of *n*-butylamine (0.1 cm³, 1.01 mmol) in chloroform (20 cm³) at 20 °C was added 1,3-bis(1-isocyanato-1-methylethyl)benzene (0.1 cm³, 0.43 mmol). The reaction mixture was left to stand under air for 24 hours at 20 °C then concentrated *in vacuo* and filtered under suction. The collected solids were washed with chloroform (2 x 20 cm³) and dried in a drying pistol. Compound **G** was obtained as a white solid (152 mg, 0.39 mmol, 90%), *m/z* (ESI-MS) 413.8 [M+Na]⁺. ¹H NMR (400 MHz, DMSO-*d*₆) δ 7.33 (t, *J* = 1.8 Hz, 1H, *h*), 7.20 – 7.08 (m, 3H, *i, j*), 6.12 (s, 2H, *f*), 5.75 (t, *J* = 5.7 Hz, 2H, *e*), 2.92 (dt, *J* = 6.3, 5.7 Hz, 4H, *d*), 1.51 (s, 12H, *g*), 1.38 – 1.18 (m, 8H, *b, c*), 0.95 – 0.73 (m, 6H, *a*). ¹³C NMR (101 MHz, DMSO-*d*₆) δ 157.59, 148.97, 127.68, 122.75, 121.75, 54.65, 38.96, 32.71, 30.63, 19.99, 14.17. Elem. Anal. Calc. (%) (C₂₂H₃₈N₄O₂) C 67.66, H 9.81, N 14.35; Found (%) C 67.40, H 9.72, N 14.27.

Preparation of Gels

Solid gelator **G** was (with or without CBZ) sonicated for 30 s in toluene followed by heating to produce a homogeneous solution. The homogenized systems were then left undisturbed at room temperature. The formation of gels was assessed by the stable-to-inversion method.

Crystal data for G

orthorhombic, space group *Pbca* (no. 61), *a* = 8.9115(2) Å, *b* = 16.2345(3) Å, *c* = 32.4328(7) Å, *V* = 4692.17(17) Å³, *Z* = 8, *T* = 120.0 K, μ (MoK α) = 0.072 mm⁻¹, *D*_{calc} = 1.106 g cm⁻³, 55636 reflections measured (5.02° ≤ 2 θ ≤ 55.0°), 5388 unique (*R*_{int} = 0.1116, *R* _{σ} = 0.0578) which were used in all calculations. The final *R*₁ was 0.0637 (*I* > 2 σ (*I*)) and *wR*₂ was 0.1738 (all data). CCDC deposition number 1851505.

SANS study

Titanium sample cells with a 1mm path length and quartz windows were preassembled and placed in a lab oven, along with needles and syringes, at 50°C for at least 10 minutes to minimize the chance of the gel forming during sample transfer. SANS samples were prepared as described above in toluene-*d*₈. Once the sample was homogenized, it was placed on a pre-heated hot plate to keep hot while the sample cell and needle and syringe were retrieved. Approximately 0.3 mL of the hot solution was injected into the sample cell, which was then capped and removed from heat. The filled cell was allowed to cool and mature overnight for at least 12 hours before being placed on the beam line.

SANS measurements were conducted at 25 °C with neutrons of wavelength $\lambda = 6$ Å and a wavelength distribution $\Delta\lambda/\lambda = 15\%$ on the NGB-30 SANS instrument¹ at the NIST Center for Neutron Scattering (NIST, Gaithersburg, MD, USA). Three sample to detector distances (SDD) were used (1.3 m, 4 m and 13.2 m) to cover the *q* range of 0.003 Å⁻¹ < *q* < 0.412 Å⁻¹, where *q* = (4 π / λ) sin(ϑ /2) (*q*=scattering vector; λ = neutron wavelength; ϑ =scattering angle). The high-*q* data at the 1.3m SDD was counted for 20 minutes, the intermediate-*q* data was counted for 40 minutes, and the low-*q* data at 13.2 m was counted for 80 minutes. The raw counts on area detector were

converted to I(q) using measurement geometry corrected for the dark current, empty cell scattering and the sensitivity of the individual detector pixels using IgorPro data reduction macros.¹¹ The corrected data were then placed on an absolute scale after normalization to the empty beam flux. The structural information was then extracted by comparing the measured cross-sections with that modeled using IgorPro and SasView software¹¹ and smeared by an instrument resolution function.

Rheology

Rheological measurements were performed using a Discovery Hybrid Rheometer DHR-1 from TA. All the gel samples were prepared in toluene at room temperature and aged for 14 h before transferring to the rheometer plate kept at 25 °C. A 40 mm cone-plate steel geometry with 55 μm truncation was used for all experiments. Stress-sweep experiments were performed at a constant frequency of 1 Hz, and the oscillation strain was increased from 0.025% to 100%. After the experiment the X-axis was converted to oscillation stress using the instrument software to better reflect the yield stress value. The frequency-sweep experiments were performed at a constant 1% strain.

SEM

A homogeneous gel sample was transferred onto the silicon wafer and the sample was immersed in liquid nitrogen before being dried *in vacuo* for 2 days. The sample was coated with platinum and investigated with SCIOS SEM/FIB.

Conflicts of interest

Authors declare no conflicts of interest.

Acknowledgements

This work was funded by start-up funds (HK) provided by Office of Research, University of Cincinnati. This work benefited from the use of the SasView application, originally developed under NSF award DMR-0520547. SasView contains code developed with funding from the European Union's Horizon 2020 research and innovation programme under the SINE2020 project, grant agreement No 654000. We thank Dr. Boualem Hommouda for valuable discussions on SANS data analyses. We thank the Engineering and Physical Sciences Research Council for a studentship (to CDJ) and the Royal Society for a Wolfson Research Merit Award (to JWS).

Notes and references

- 1 D. K. Kumar, J. W. Steed, *Chem. Soc. Rev.*, 2014, **43**, 2080.
- 2 (a) D. Erdemir; A. Y. Lee and A. S. Myerson, *Acc. Chem. Res.* 2009, **42**, 621; (b) P. G. Vekilov, In *Physics of Complex Colloids*; Bechinger, C.; Sciortino, F.; Zihnerl, P., Eds., 2013; Vol. 184.
- 3 Representative reviews on crystallization: (a) D. Gebauer, M. Kellermeier, J. D. Gale, L. Bergstrom and H. Colfen, *Chem. Soc. Rev.*, 2014, **43**, 2348; (b) S. Jungblut and C. Dellago, *Eur. Phys. J. E*, 2016, **39**, 77; (c) F. Schuth, *Curr. Opin. Solid State Mater. Sci.*, 2001, **5**, 389; (d) D. Mangin, F. Puel, and S. Veessler, *Org. Process Res. Dev.*, 2009, **13**, 1241; (e) J. Nyvlt, *Orog. Crystal Growth and Charact.* 1984, **9**, 335; (f) A. Mersmann and M. Löffelmann, *Chem. Eng. Technol.*, 2000, **23**, 11.
- 4 Representative reviews on supramolecular gels: (a) P. Terech and R. G. Weiss, *Chem. Rev.*, 1997, **97**, 3133; (b) N. M. Sangeetha and U. Maitra, *Chem. Soc. Rev.*, 2005, **34**, 821; (c) M-O. M. Piepenbrock, G. O. Lloyd, N. Clarke and J. W. Steed, *Chem. Rev.*, 2010, **110**, 1960; (d) A. Dawn, T. Shiraki, S. Haraguchi, S. Tamaru and S. Shinkai, *Chem. Asian J.* 2011, **6**, 266; (e) B. O. Okesola and D. K. Smith, *Chem. Soc. Rev.*, 2016, **45**, 4226; (f) C. D. Jones, J. W. Steed, *Chem. Soc. Rev.* 2016, **45**, 6546; (g) A. Dawn and H. Kumari, *Chem. Eur. J.*, 2018, **24**, 762.
- 5 (a) J. A. Foster, M-O. M. Piepenbrock, G. O. Lloyd, N. Clarke, J. A. K. Howard and J. W. Steed, *Nat. Chem.* 2010, **2**, 1037; (b) A. Dawn, K. S. Andrew, D. S. Yufit, Y. Hong, J. P. Reddy, C. D. Jones, J. A. Aguilar, and J. W. Steed, *Cryst. Growth Des.* 2015, **15**, 4591; (c) L. Kaufmann, S. R. Kennedy, C. D. Jones and J. W. Steed *Chem. Commun.*, 2016, **52**, 10113; (d) J. A. Foster, K. K. Damodaran, A. Maurin, G. M. Day, H. P. G. Thompson, G. J. Cameron, J. C. Bernal and J. W. Steed, *Chem. Sci.*, 2017, **8**, 78.
- 6 (a) H. Inomata, S. Goto, K. Otake and S. Saito, *Langmuir*, 1992, **8**, 687; (b) A. R. Hirst and D. K. Smith, *Chem. Eur. J.*, 2005, **11**, 5496. (c) L. E. Buerklea and S. J. Rowan, *Chem. Soc. Rev.*, 2012, **41**, 6089; (d) S. M. Ramalheite, K. P. Nartowski, N. Sarathchandra, J. S. Foster, A. N. Round, J. Angulo, G. O. Lloyd and Y. Z. Khimyak, *Chem. Eur. J.*, 2017, **23**, 8014.
- 7 (a) D. J. Cornwell and D. K. Smith, *Mater. Horiz.*, 2015, **2**, 279; (b) D. Dasgupta, S. Srinivasan, C. Rochas, A. Ajayaghosh and J. M. Guenet, *Langmuir*, 2009, **25**, 8593.
- 8 (a) P. Terech, D. Pasquier, V. Bordas and C. Rossat, *Langmuir*, 2000, **16**, 4485; (b) P. Terech, A. Coutin and A. M. Giroud-Godquin, *J. Phys. Chem. B*, 1997, **101**, 6810; (c) M. George, G. P. Funkhouser, P. Terech and R. G. Weiss, *Langmuir*, 2006, **22**, 7885; (d) R. A. Hule, R. P. Nagarkar, A. Altunbas, H. R. Ramay, M. C. Branco, J. P. Schneider and D. J. Pochan, *Faraday Discuss.*, 2008, **139**, 251 (e) J-B. Guilbaud and A. Saiani, *Chem. Soc. Rev.*, 2011, **40**, 1200; (f) H. Kumari, S. E. Armitage, S. R. Kline, K. K. Damodaran, S. R. Kennedy, J. L. Atwood and J. W. Steed, *Soft Matter*, 2015, **11**, 8471; (g) H. Kumari, S. R. Kline, S. R. Kennedy, C. Garvey, C. L. Raston, J. L. Atwood and J. W. Steed, *Chem. Commun.*, 2016, **52**, 4513; (h) I. W. Hamley, S. Burholt, J. Hutchinson, V. Castelletto, E. Rodrigo da Silva, W. Alves, P. Gutfreund, L. Porcar, R. Dattani, D. Hermida-Merino, G. Newby, M. Reza, J. Ruokolainen and J. Stasiak, *Biomacromolecules*, 2017, **18**, 141; (i) L. L. E. Mears, E. R. Draper, A. M. Castilla, H. Su, Zhuola, B. Dietrich, M. C. Nolan, G. N. Smith, J. Douth, S. Rogers, R. Akhtar, H. Cui and D. J. Adams, *Biomacromolecules*, 2017, **18**, 3531.
- 9 J. Buendia, E. Matesanz, D. K. Smith and L. Sanchez, *CrystEngComm* 2015, **17**, 8146.
- 10 M. Lang, J.W. Kampf and A. J. Matzger, *J. Pharm. Sci.*, 2002, **91**, 1186.
- 11 J.-B. Arlin, L. S. Price, S. L. Price and A. J. Florence, *Chem. Commun.* 2011, **47**, 7074.
- 12 (a) J. H. van Esch, F. Schoonbeek, M. de Loos, H. Kooijman, A. L. Spek, R. M. Kellogg and B. L. Feringa, *Chem. Eur. J.* 1999, **5**, 937; (b) M. de Loos, A. Friggeri, J. van Esch, R. M. Kellogg and B. L. Feringa, *Org. Biomol. Chem.* 2005, **3**, 1631; (c) F. Fages, F. Vögtle and M. Žinic, In *Top. Curr. Chem.*, 2005; Vol. 256; (d) M. O. M. Piepenbrock, G. O. Lloyd, N. Clarke and J. W. Steed, *Chem. Commun.* 2008, 2644.

- 13 (a) S. Kline, *J. Appl. Crystallogr.*, 2006, **39**, 895; (b) <http://www.sasview.org/>
- 14 Roe, R. J. *Methods of X-ray and Neutron Scattering in Polymer Science*; Oxford University Press: New York, 2000
- 15 (a) J. Ryu, J. Ko, H. Lee, T.-G. Shin, and D. Sohn, *Macromolecules*, 2016, **49**, 1873; (b) H. Wang, W. Zhou, D. L. Ho, K. I. Winey, J. E. Fischer, C. J. Glinka, E. K. Hobbie, *Nano Letters*, 2004, **4**, 1789; (c) D. W. Schaefer, J. M. Brown, D. P. Anderson, J. Zhao, K. Chokalingam, D. Tomlin, J. Ilavsky, *J. Appl. Cryst.*, 2003, **36**, 553; (d) S. Mallam, F. Horkay, A.-M. Hecht, A. R. Rennie, and E. Geissler, *Macromolecules*, 1991, **24**, 543; (e) M. Shibayama, T. Tanaka, C. C. Han, *J. Chem. Phys.*, 1992, **97**, 6829; (f) M. Shibayama, H. Kurokawa, S. Nomura, M. Muthukumar, R. S. Stein, S. Roy, *Polymer*, 1992, **33**, 2883
- 16 G. Yu, X. Yan, C. Han and F. Huang, *Chem. Soc. Rev.* 2013, **42**, 6697.
- 17 G. M. Sheldrick, *Acta Crystallogr. Sect. C* 2015, **71**, 3.
- 18 O. V. Dolomanov, L. J. Bourhis, R. J. Gildea, J. A. K. Howard and H. Puschmann,, *J. Appl. Crystallogr.* 2009, **42**, 339.